Enhanced proton acceleration using hollow silica nano-sphere coated targets

Rakesh Y. Kumar (iD), Baljeet Singh (iD), M. Kundu, Pankaj Kumar Rastogi (iD), Sheroy Tata, V. Rakesh Kumar (iD), Amit D. Lad (iD), Yesh M. Ved, R. Gopal (iD), V. Sharma (iD), and M. Krishnamurthy (iD)

View Online   Export Citation   CrossMark

ARTICLES YOU MAY BE INTERESTED IN

Enhanced proton acceleration using hollow silica nano-sphere coated targets

View Online   Export Citation   CrossMark

Rakesh Y. Kumar,[1,2] Baljeet Singh,[2] M. Kundu,[3,4] Pankaj Kumar Rastogi,[2] Sheroy Tata,[5]
V. Rakesh Kumar,[5] Amit D. Lad,[5] Yesh M. Ved,[5] R. Gopal,[2] V. Sharma,[1] and M. Krishnamurthy[2,5,a]

AFFILIATIONS

[1]Indian Institute of Technology, Hyderabad, Kandi, Telangana 502285, India
[2]TIFR-Center for Interdisciplinary Sciences, Hyderabad, Gopanpally, Serlingampalli, Telangana 500107, India
[3]Institute of Plasma Research, Bhat, Gandhinagar 382428, India
[4]Homi Bhabha National Institute, Training School Complex, Anushakti Nagar, Mumbai 400094, India
[5]Tata Institute of Fundamental Research, Homi Bhabha Road, Navy Nagar, Colaba, Mumbai 400005, India

[a]Author to whom correspondence should be addressed: mkrsim@tifr.res.in

ABSTRACT

Acceleration of protons by transient strong electric fields formed with intense ultrashort laser pulses is important for advancements in radiography and biomedical applications. Controlling the absorption mechanisms by material modification or adding structural features to the solid substrate is important to enhance ion energies for a given laser intensity. We present here an experimental demonstration of enhanced proton acceleration when a BK-7 glass target is coated with 150 nm diameter silica hollow spheres. The hollow particle coated target yielded a maximum proton energy of ≥ 800 keV at a peak intensity of 10^{18} W cm^{-2} while the maximum energy is only up to 200 keV with a plain glass target under otherwise identical conditions. Two-dimensional particle in cell simulations demonstrate the role of local fields in the hollow spherical cavities that lead to the enhanced proton energies comparable to the experiments.

I. INTRODUCTION

When an intense ultrashort laser impinges on any substrate, instantaneous ionization of atoms followed by electron heating leads to a hot dense high temperature plasma. At intensities $\geq 10^{14}$ W cm^{-2}, most atoms undergo tunnel or over barrier ionization.[1] Electrons continue to interact with the incident laser fields and experience both collisional and collisionless absorption[2] depending on the target geometry and laser pulse parameters. Prominent laser absorption mechanisms include vacuum heating,[3] resonance absorption,[4] anomalous skin effect,[5] and $\vec{J} \times \vec{B}$ heating.[6] Ponderomotive drive by the incident fields and quasi-static electric fields generated by the plasma density gradients result in a hot electron temperature as large as a few hundred keV energy and steep plasma density gradients.[7,8]

Hot electrons cross the target surface and create a charge separated sheath potential[9] that is as large as a few TV/m.[10] This large quasi-static field leads to ion acceleration. Protons have the lowest mass/charge ratio for the ions. They acquire a much larger velocity than any other ions and are the fastest to leave the target surface. Since the laser energy is deposited in a few micrometers area, both electron and ion emission have a low spatial source size. The ultrashort nature of the burst leads to a compact, high brightness source of electron beams, ion beams (especially protons and carbons), neutral atoms, and x-ray beams. Such particle beams have potential applications in fast ignition schemes,[11–13] proton radiography,[14] streak deflectometry,[15] and generation of medical isotopes.[16]

The physics of intense laser matter interaction, depends on the type of target (gas, solids, mass limited targets) and various laser parameters (intensity, pulse duration, etc.).[17] For a thick solid target, hot electrons leave along a direction normal to the target and the transient field generated at the target surface leads to backward emission of ions. For a very thin target, hot electrons also leave at the rear side target and ion acceleration is possible both at the target rear and the front side, where the laser is incident. A large volume of work studying proton acceleration from laser solid interactions[18,19] exists in the literature. Rear side proton acceleration studies are usually performed with a few micrometer thick foil targets wherein high quality proton beams with MeV energies[20,21] are produced. On the other hand, the front side ion energies are never as high as the rear side. Expansion of the

electron density at the target front brings down the sheath potential and consequently lowers ion acceleration. Front side proton energies are $<200\,keV$ at 10^{18} W cm^{-2} with plain solid metal targets.[22] Front side acceleration schemes are, however, important to study the effect of surface modifications on the ion acceleration. Surface modifications such as nanoparticle coating, foam coating, and micro-/nanopores on the target enhance the absorption of laser energy[23] and the resultant particle acceleration.[24–27] Phenomena such as enhanced laser energy absorption beyond the skin depth due to nanoparticles[28,29] or laser excited surface waves that enhance the local electric field,[30] are notable. Anharmonic heating of electrons leading to enhanced electron and proton energy[31–33] by microparticle coatings has also been shown to contribute to efficient particle acceleration.

In this context, a coating of spherical hollow nano-particles on a substrate is a novel target surface modification. Considering an isolated nano-particle, with a large number of surface atoms compared to the core, larger transient electrostatic field gradients are possible. All ions on the spherical surface will experience a uniform potential,[34–36] so mono-energetic features in the ion acceleration can also be anticipated. The present study explores the possibility of enhancement in proton generation utilizing hollow nano-spheres. We demonstrate that up to 800 keV protons are generated with a hollow particle coated target where the maximum energy is only about 200 keV with the plain target. 2D-particle in cell (PIC) simulations show that electron depletion from the hollow spherical shell leads to sharper transient electrostatic field gradients. Both the electron energies and proton energies are larger with the hollow particle coated targets and the simulated proton spectra correlate well with the experimental measurements.

II. EXPERIMENT

The laser facility at the Tata Institute of Fundamental Research, Mumbai, is operated at 40 TW. A P-polarised, 500 mJ, 800 nm, and 25 fs laser pulse is routed onto a target and focused at 45° to the target normal with an f/3.5 off-axis parabolic mirror (OAP) to generate an intensity of 2×10^{18} W cm^{-2} on the target. The focal waist of the beam is 30 μm in diameter (FWHM) and contains 63% of the beam energy (500 mJ). Figure 1(a) illustrates the experimental schematic. The target placed in a vacuum chamber maintained at 10^{-5} Torr pressure is rastered with X and Y translation stages such that each laser shot is incident on a fresh spot of the target substrate. Ion emission is sampled through a 100 μm aperture placed at 63.8 cm from the laser focus at the target normal and diagnosed using a Thomson Parabola Ion Spectrometer (TPIS).[37] Ions deflected by parallel electric and magnetic fields are detected on a microchannel plate (MCP) (F2225–21 PGF) that is kept at 1.36 m from the target. MCP is coupled to a P43 phosphorus screen and the ion splat position is recorded with a 12-bit CoolSnap HQ CCD camera. Ions of given m/q form a parabolic trace. The undeflected neutral atoms and photons strike at the origin of the spectrogram. The lower the energy of the ions, the higher the deflection is, so the highly energetic ions strike closer to the central spot. The
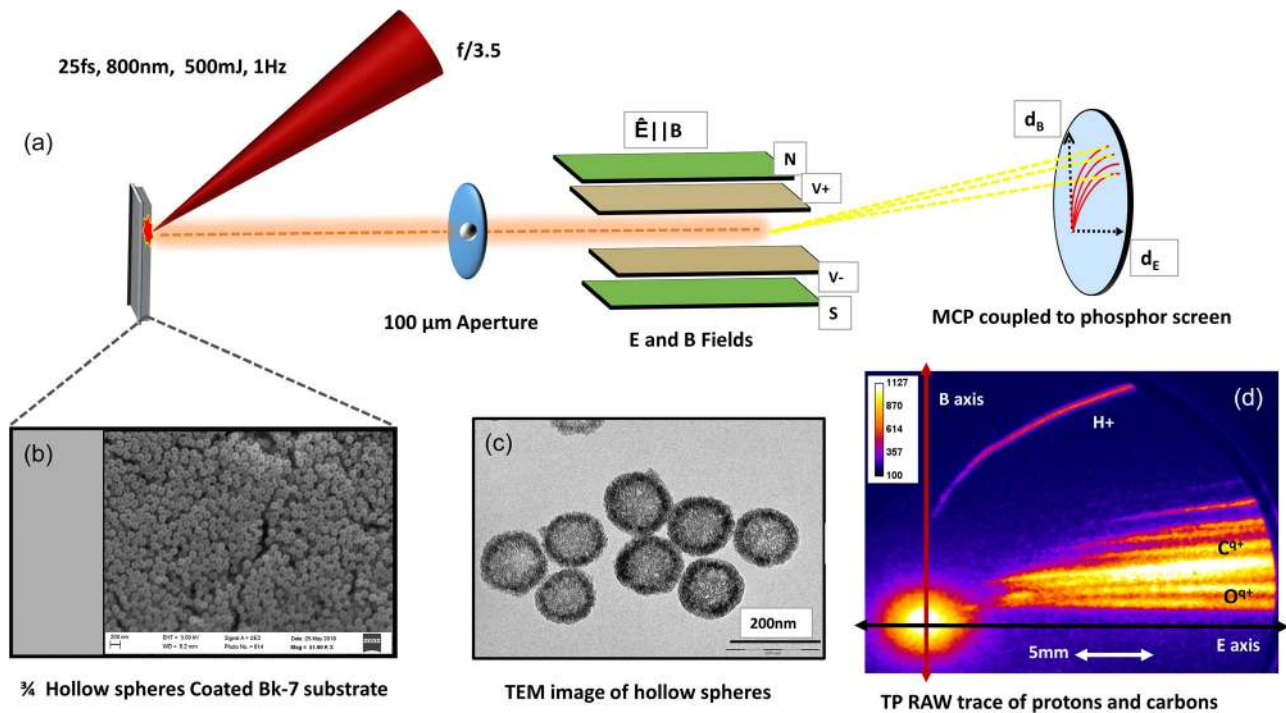

FIG. 1. (a) Experimental setup: a 500 mJ laser beam is focused on a 3 mm thick solid target at 45° to the target normal and ion emission at 10^{18} W cm^{-2} is studied using a Thomson Parabola Ion Spectrometer either on a $\lambda/$ 10 polished BK-7 glass or the same substrate coated with 150 nm hollow spherical particles. (b) Scanning electron microscope image of the dense particle coated target. Top view depicts that the spin coating results in a uniform layer of hollow particles and the variation in the thickness is about one monolayer. (c) A high resolution transmission electron microscope image gives a magnified view of a single nano-particle of size 150 ± 10 nm and a shell thickness of 30 nm. (d) A TP spectrum of ion emission from the plain glass target with low dispersion fields in the TP, shows well resolved parabolic ion traces. Ion energy spectra extracted from the image are shown separately.

magnetic field and electric field are varied to resolve traces of different ion species and also to obtain the kinetic energy. The Thomson Parabola (TP) spectrum from a plain solid target is shown in Fig. 1(d). Protons and different charge states of carbon and oxygen are resolved. By switching off the electric field, ions are dispersed along the axis labeled B-axis. Similarly, the magnetic field is switched off to deflect the ions along the E-axis. Using the axes and the parabolic equations of ion motion, charge resolved ion spectra are derived from the TP images. We note that the noise in the image varies non-linearly from the point away from the origin. We follow a detailed noise analysis elaborated in our earlier work.[38] The signal at the origin is largely due to the neutral atoms and is different for the plain glass target and the nano-particle coated target. The extracted ion energy spectrum takes note of the noise corrections and is not influenced by the change in the signal at the origin.

Hollow silica nanoparticles (HSN-150) were synthesized using an established procedure[39] with some minor modifications. 20 mg of HSN-150 was mixed in 2 ml of ethanol and sonicated for 10 min. The mixture was vortexed for 5 min and 5 layers of HSN-150 solution were coated on a 3 mm thick $\lambda/10$ polished BK-7 glass substrate using a spin coating technique in a clean room. A quarter of the substrate was left uncoated for experimental convenience so as to compare the experimental results with the coated and uncoated targets under otherwise identical conditions. The Scanning Electron Microscope (SEM) image of the substrate is shown in Fig. 1(b) and and indicates that the coating is uniform to variation of up to one mono-layer of the nano-particles. The thickness of the coating is larger than the skin depth and so essentially the laser energy is deposited in the nano-particle coating. The target is rastered and the laser pulse irradiation is done over several fresh portions of the target to measure the proton emission to include the changes in the target coating thickness. The large changes in the proton emission due to coating reported here are beyond the variations that may occur due to the changes in coating thickness. The transmission electron microscope (TEM) image of individual HSN-150 particles with a high resolution is also shown in Fig. 1(c). HSN-150 particles have a very uniform diameter of 150 nm ± 10 nm and the shell thickness is about 30 nm. A comparison of the ion spectra extracted from the TPIS is used to decipher the effect of the particle coating on ion acceleration.

III. RESULTS AND DISCUSSION

Figure 2(a) shows the proton spectrum with very low dispersion fields in the TP (150 Gauss magnetic field and 20 V/cm of electric field) with the uncoated BK-7 target. The ion energies are below 100 keV. In these conditions, the proton parabola is not fully separated from the central spot. Even with larger dispersion fields, the proton energies are at best 200 keV with the plain glass target. We emphasize that, for similar intensities with the use of ($<5\,\mu$m) foil as the target and at the rear side, we do observe the proton spectrum with the maximum energy extended to 2–5 MeV.[37] For experiments with low dispersion fields in TPIS, the low energy proton spectra shows no difference with the HSN-particle coating, as shown in Fig. 2(b). However, when the fields in the TPIS are increased to separate the protons from the central spot, the proton spectrum is very different with and without the HSN-150. Figure 3 demonstrates the results of such an experiment. As anticipated, we find that the major changes are associated with the proton spectrum and especially at the higher energy end of the proton spectrum. So, the E and B fields of the

spectrometer are changed so that the higher energy components in the proton spectrum are well resolved. As can be seen in Fig. 3(b), a zoom into the high energy proton spectral region, there is a clear trace of high energy protons only when the laser is impinged on the HSN coated target. Figure 3(c) shows the same region of the spectrum with the plain glass target. There is barely a discernible signal of the protons in this energy range. Figure 3(a) shows the proton energy spectrum derived from the raw images shown in Figs. 3(b) and 3(c). The red circles in the spectrum give a measure of the weak signal above the background in the same region of the spectrum for the plain glass target. The proton signal in the 150–1000 keV energy range is very low in the absence of the HSN coating and signal-to-noise ratio is poor due to the weak signal. The interference from the neutral atom spot is larger at the high energy end and this shows up as increased signal in the plot. On the other hand, the HSN-150 coated target clearly shows proton emission with energies as large as 800 keV. The high energy proton yield is large and is not influenced by the signal at the central spot. We note that there are no significant changes in the heavy ion spectra with the increase in the TP fields. The maximum ion energy of the O^+ is the same with or without particle coating, though the O^+ ion yield is larger with the particle coating. Figures 2(c) and 2(d) show the O^+ spectrum with low and high dispersion fields. Since the parabolae are well separated from the spot at the origin, there is very little difference. The low energy ions (<80 keV) are presumably due to the hydrodynamic pressure and do not change much with the particle coating. The higher energy protons driven by the sheath field are however influenced by the particle coating.

For the over dense plasmas possible with solid targets; laser intensity, polarization, pulse contrast, and pre-plasma scale length control the mechanism for electron acceleration. Based on various experiments, models, and calculations, the temperature scaling of hot electrons is related to the ponderomotive scaling as $E_e \sim m_e c^2\left(\sqrt{1 + a_0^2/2} - 1\right)$,[40] where a_0 is the normalized peak strength of the laser given by $a_0 = \sqrt{I/I_0 \cdot \lambda^2}$ and I, the peak laser intensity in units of W/cm^2, and λ is the driving laser wavelength in μm, $I_0 = 1.37 \times 10^{18}$ W/cm^2. The generation of relativistic electrons requires relativistic laser intensities of the order of $a_0 > 1$, i.e., $I > 2 \times 10^{18}$ W/cm^2 for wavelength 800 nm. The self-consistent sheath electric field from the isothermal plasma expansion model can be estimated to be, $E_0 = \left(\sqrt{n_0 * K_B * T_e/\epsilon_0}\right)$ with n_0 being the maximum electron density, K_B Boltzmann constant, T_e the hot electron temperature, and ϵ_0 the permittivity of free space. Clearly, the quasi-static field that accelerates the ions depends strongly on the electron density and hot electron temperature. Modifications of the target surface change the local fields and the plasma scale length which affect the absorption of the laser pulses. Both the electron temperature and effective electron density change the quasi-static sheath potential and subsequently the maximum electron energy. A fourfold increase in the maximum ion energy would require a 16-fold increase in the ($n_0 * T_e$). To evaluate the changes in plasma generation and to correlate with the experimental measurements, we perform fully relativistic 2D-3 V electromagnetic PIC simulations. The PIC code used by us is a suite of programs developed by one of the co-authors for laser plasma interaction studies (in 3D, 2D, 1D). Necessary details of the PIC simulation and its usage are elaborated in our earlier studies.[31–33]
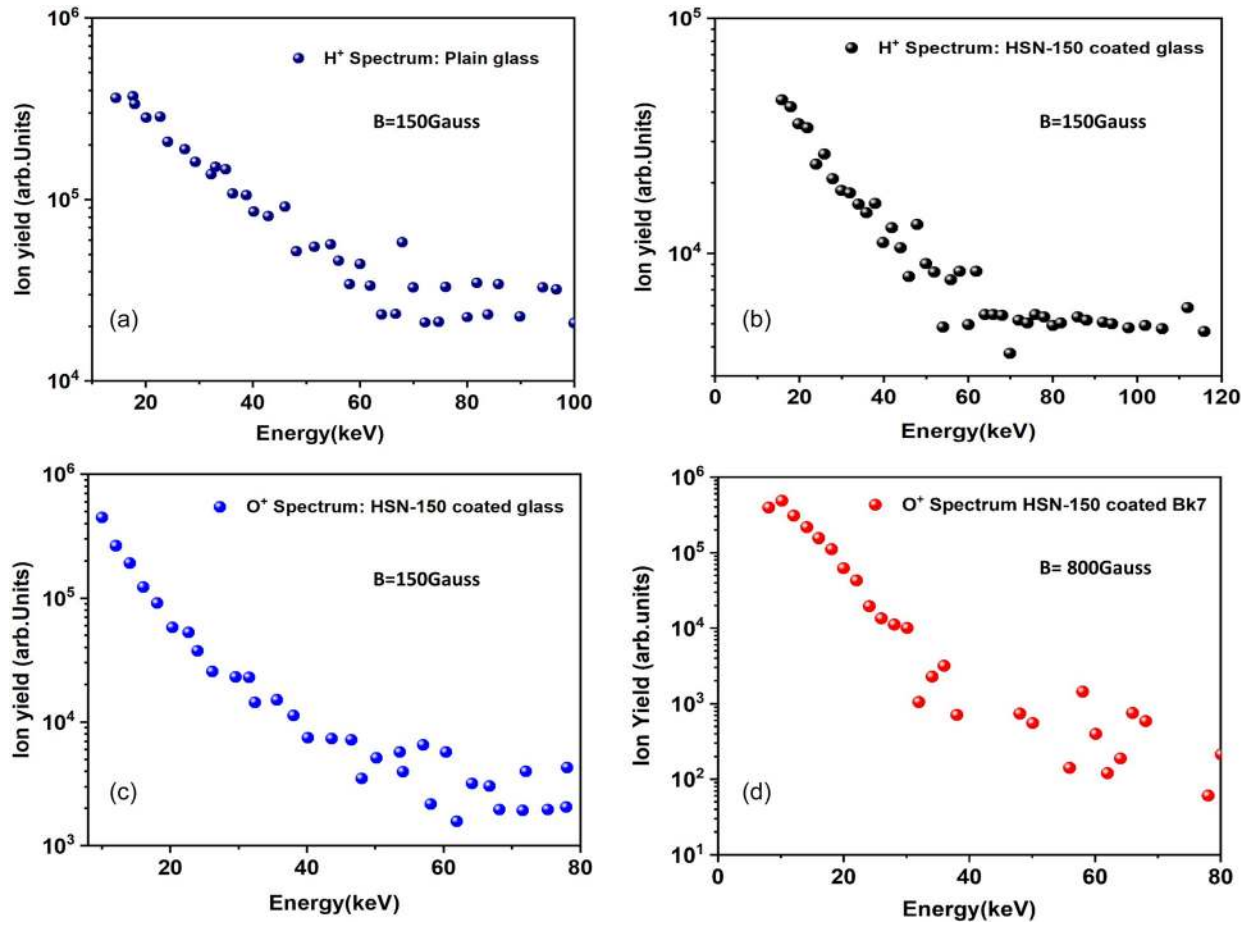
FIG. 2. (a) Proton spectrum for the uncoated plain BK-7 glass and (b) proton spectrum with HSN-150 particle coating. Here, the dispersion fields in TPIS are low and the proton trace is not well separated from the central spot. Higher dispersion fields are mandatory to separate the proton trace away from the neutral atom spot at the center. [(c) and (d)] Oxygen ion spectrum with the HSN-150 particle coating with low and high dispersion fields, respectively. Unlike the proton spectrum, even in the low fields, the ion trace is well separated from the spot at the origin and increase in TPIS dispersion fields does not change the ion spectrum.

In the PIC simulation, we simulate two different target configurations irradiated by a laser pulse of wavelength $\lambda = 800$ nm mimicking the experiments: (i) a slab substrate of (transverse $\times$ longitudinal) dimension $L_x \times L_y \sim 20\lambda \times 2\lambda$ and (ii) the same slab substrate on which a number of hollow-spherical particles (outer diameter 150 nm and shell-thickness 40 nm) are placed close to each other along the target-front surface. We use a uniform numerical grid resolution of 40 grids per wavelength ($\Delta = \lambda/40$) in the PIC simulation for the convergence of numerical results and negligible numerical heating. For $\lambda = 800$, it gives grid size $\Delta = 20$ nm and a shell thickness of 40 nm will cover two grids fully. However, with this resolution, a 30 nm shell will cover only 1.5 grids and the field and particle dynamics within the shell will be less resolved. One may argue that a grid size of $\Delta = \lambda/80 = 10$ nm would be even better in the simulations, and in this case, we can take an exact 30 nm shell as in experiments. But that increases the computational burden 20–25 times, which is unaffordable. Since the aim of the calculations is to probe the local field effects, the inferences drawn from the computations are not erroneous.

Both the slab-substrate and hollow-spheres are assumed with electron density $n_e \approx 20n_c$, neutralizing the ion (proton) background at the initial time, where $n_c \approx 1.72 \times 10^{21}$ cm^{-3} is the critical density at 800 nm. The choice of n_c is based on prior experience with simulations on nano-/microparticle coatings.[31–33] Since experiments were performed with a 25 fs (FWHM) laser pulse (for which total duration is approximately 66 fs), we have kept the same duration for simulations. Simulations are performed on a computational box having 1000×1000 uniform rectangular grids with size $\Delta x = \Delta y = \lambda/40$. A uniform time step of $\Delta t = \Delta y/2c$ (c is the speed of light in a vacuum) is chosen to ensure energy conservation and negligible numerical heating. The target is rotated in the incident x–y plane about the vertical z-axis to control the angle of incidence of the laser so that the center of the target coincides with the center of the simulation box. The laser is assumed to be a p-polarized Gaussian beam of focal width $w_0 = 15\lambda$ with the transverse electric field as $E_x(t, x, y = y_l) = E_0(w_0/w(y))\exp(-r^2/w(y)^2) \times \mathrm{Re}[\exp(i\omega(t - y/c)) + i\arctan(y/y_R) - i\omega r^2/2cR(y)]$ which is numerically excited at the left longitudinal end $y = y_l$ and propagated across the computational box to the right in the
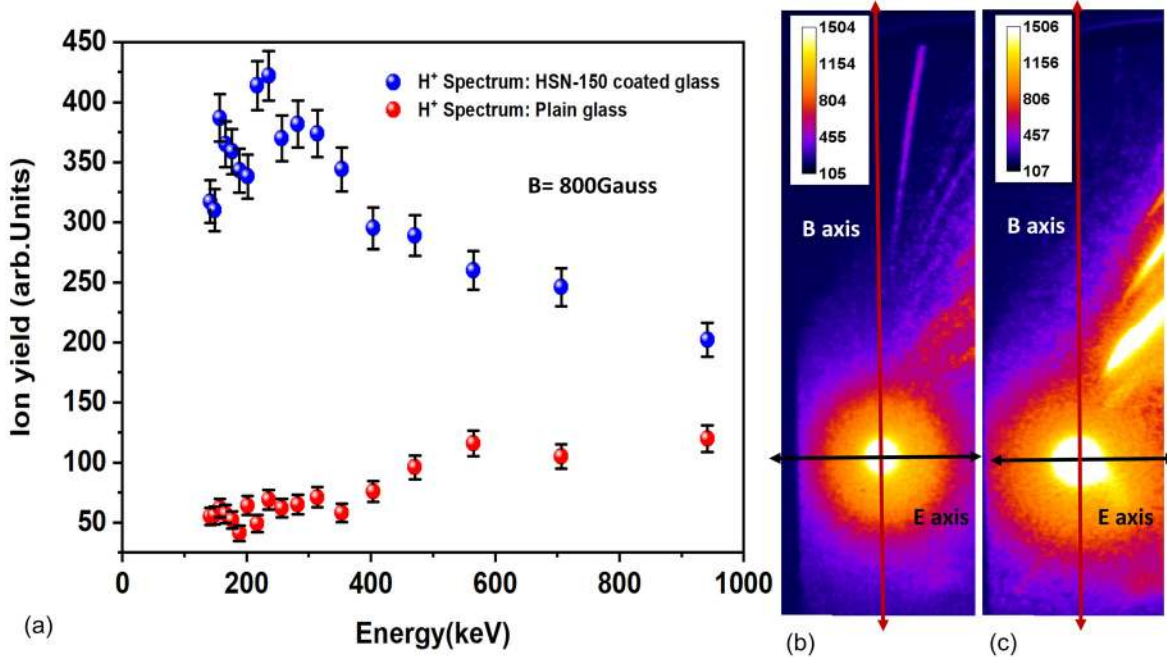
FIG. 3. (a) TPIS proton spectrum with larger TPIS dispersion fields with and without the HSN-150 coating. Higher proton energy with the particle coating is clear (see the text). TPIS images for both the nano-sphere coated target (b) and the plain target (c) at the relevant portion are shown.

+y-direction, where $y_R = \omega w_0^2/2c$ is the Rayleigh range and $R(y) = y + y_R^2/y$ is the radius of curvature of the beam. The peak intensity, pulse width, and angle of incidence of the laser beam are taken as close as to the experiment: 3.5×10^{18} W/cm^2, 25 fs, and 45°, respectively. Figure 4 shows the essential results of the simulations after the end of the laser pulse, i.e., at ~66 fs. The large number of particles used in the simulation imply that the particle emission should follow Poisson statistics and the error in electrons/protons with N counts scales as sqrt(N). The key point of the plots is not the absolute value of the electron/proton yield but the differences in the emission compared to the plain solid target. Only the statistically significant differences are discussed in understanding the changes in plasma with the nano-particle coating.

For a plain slab target, as shown in Fig. 4(a), the electron spectrum shows two temperatures. The higher temperature at about 1.3 MeV is very low in yield. But, in the presence of hollow-spherical particles, the higher energy component is clearly present. A differential electron density plot ($n_e - n_{e0}$, with respect to the initial density n_{e0}) given in (c) clearly shows that the shell region of each hollow-spherical particle has a significant electron density depletion by $\approx 15 n_c$, while the void region has a significant electron density enhancement by $\approx 20 n_c$ (see also the projection in the inset). These highly localized density structures at the target front, cause a sharp transient quasi-static potential gradient that can accelerate the protons with enormous energies from the target front. The resulting proton spectra with and without the hollow particles are shown in Fig. 4(b). The proton spectrum shows three temperature components. The lowest temperature at about 18 keV and is anticipated to be due to the Hydrodynamic forces in the plasma. The second temperature component at about 70 ± 5 keV is due to the sheath field developed at the plain target

surface. While the low energy part of the spectrum is similar to that with the plain slab, there is clearly a high energy component in the proton emission that extends to about 1.3 MeV when there is a hollow-spherical particle coating on the slab. The high energy component is due to the local fields formed only when there is nano-particle coating at the target and shows enhanced coupling of laser energy with the HSN. The induced quasi-static (transient) longitudinal electric fields E_y (in units of 5.14×10^{11} V/m) due to density spikes in-and-around the hollow-spherical nano-particles are clearly visible in the panel Fig. 4(d). Here, the corresponding induced fields for the plain slab case are subtracted from those in the case of the coated slab for better visibility. The maximum value of the induced field is $E_y^{max} \approx 4 \times 10^{12}$ V/m in the panel of Fig. 4(d). For a crude estimation of proton energies, an average field $E_y^{avg} \approx 2 \times 10^{12}$ V/m may be assumed to act during the interaction time ($\tau \approx 66$ fs) in the case of hollow-spherical particles. It gives an estimate of the maximum proton energy $\mathcal{E} \approx (q_p E_y^{avg} \tau)^2 / m_p \approx 1.1$ MeV close to the simulation results in panel (b) and correlates with the experiments fairly well, although the simulated maximum proton energy is slightly higher than the experimental data. Thus, the enhanced proton energy is attributed to the changes in local fields and indicates better coupling of incident laser energy.

IV. CONCLUSIONS

To summarize, coating a plain solid slab target with a few layers of 150 nm hollow spherical particles enhances the plasma temperature and the electron density responsible for the formation of the sheath potential on the surface of the target. Measurement of the proton energy at the front side of the target, where the laser energy is
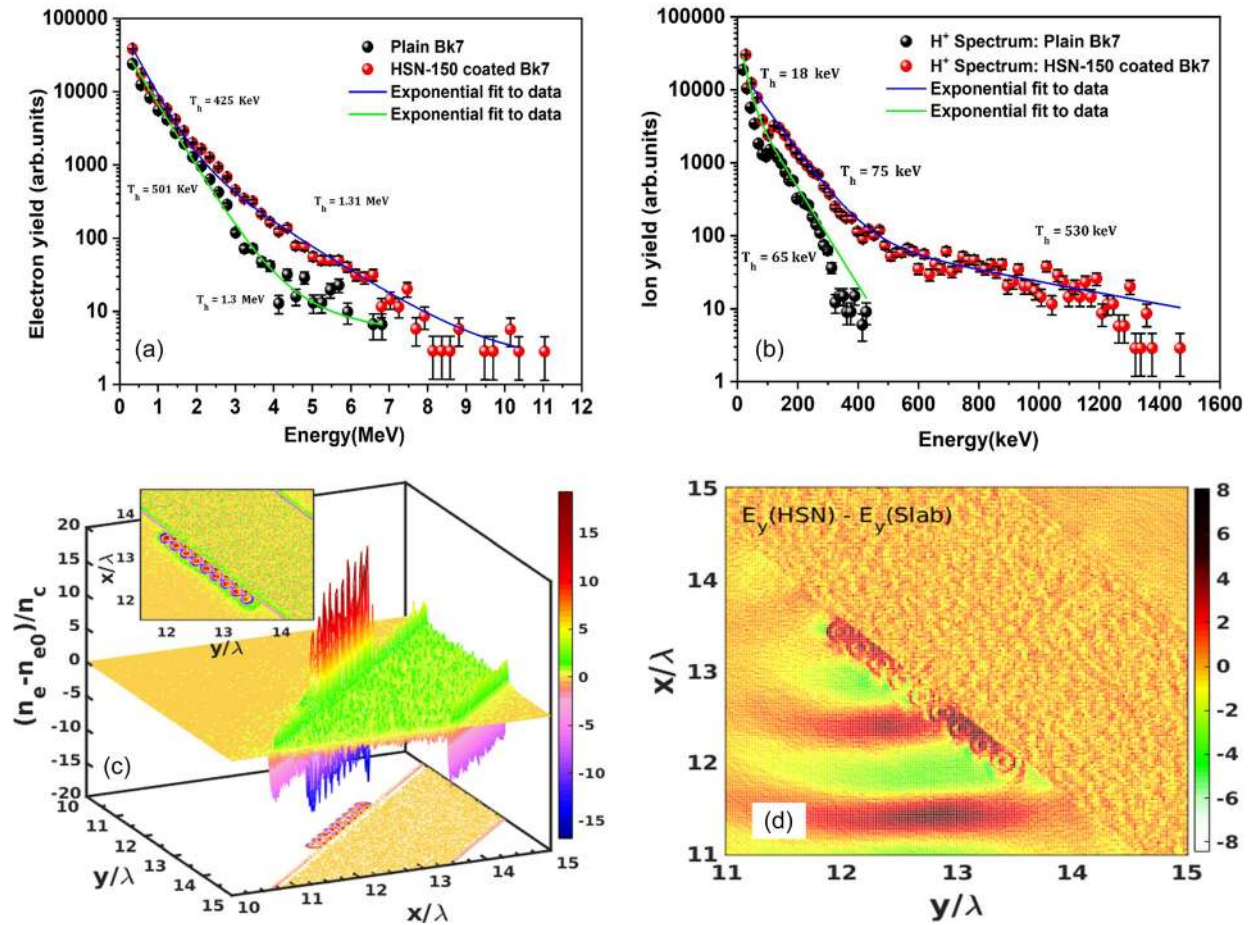
FIG. 4. Spectra of (a) electron energy and (b) proton energy obtained by fully relativistic 2D-PIC simulations after 66 fs of interaction of a 800 nm, 25 fs, p-polarized Gaussian laser beam of intensity 3.5×10^{18} W/cm² with (i) a slab target of dimension $20\lambda \times 2\lambda$ and (ii) the same slab-substrate with hollow-spherical particles (outer diameter 150 nm and shell-thickness 40 nm) placed along the slab-front. Both the slab and hollow-spheres are assumed with electron (proton) density $n_e \approx 20 n_c$ at $t = 0$, where $n_c \approx 1.72 \times 10^{21}$ cm⁻³. (c) Differential electron density ($n_e - n_{e0}$, with respect to the initial density n_{e0}), highlighting the creation of a huge density gradient (see also projection in the inset); and (d) the corresponding enhanced quasi-static longitudinal electric fields E_y (in units of 5.14×10^{11} V/m) responsible for enhanced proton energies due to the density spikes in-and-around the hollow-spherical nano-particles are clearly visible. See the text for details.

deposited, provides a very good demonstration of this effect. Proton energy measurements are carried out using high contrast, 25 fs laser pulses focused to 10^{18} W/cm² on a plain glass target either with hollow particle coating or on a (uncoated) plain solid slab. While the plain, solid target yields a <200 keV proton energy, the hollow particle coated portion of the target yields a maximum proton energy that is extended to about 800 keV. 2D-PIC simulations show that the hollow particle coating leads to a component of electrons with an enhanced temperature of about 1.3 MeV. The laser irradiation on the hollow particles therefore results in an electron depleted spherical sheath. The electron density varies sharply between the void and the shell of the hollow particle. Both the enhanced electron temperature and the higher electron density gradient result in an enhanced sheath potential and increased high energy proton emission. The proton spectrum simulated in the PIC simulations clearly shows the generation of a high energy proton component that is possible with the hollow spherical coated target.

DATA AVAILABILITY

The data that support the findings of this study are available from the corresponding author upon reasonable request.

REFERENCES

[1]P. Gibbon, *Short Pulse Laser Interactions With Matter: An Introduction* (Imperial College Press, 2005).

[2]P. Gibbon and A. R. Bell, Phys. Rev. Lett. **68**, 1535 (1992).

[3]F. Brunel, Phys. Rev. Lett. **59**, 52 (1987).

[4]J. P. Freidberg, R. W. Mitchell, R. L. Morse, and L. I. Rudsinski, Phys. Rev. Lett. **28**, 795 (1972).

[5]E. S. Weibel, Phys. Fluids **10**, 741 (1967).

[6]W. L. Kruer and K. Estabrook, Phys. Fluids **28**, 430 (1985).

[7]S. C. Wilks, W. L. Kruer, M. Tabak, and A. B. Langdon, Phys. Rev. Lett. **69**, 1383 (1992).

[8]S. C. Wilks and W. L. Kruer, IEEE J. Quantum Electron. **33**, 1954 (1997).

[9]P. Mora, Phys. Rev. Lett. **90**, 185002 (2003).

[10]I. Blumenfeld, C. E. Clayton, F. J. Decker, M. J. Hogan, C. Huang, R. Ischebeck, R. Iverson, C. Joshi, T. Katsouleas, N. Kirby et al., Nature **445**, 741 (2007).

[11]M. Tabak, J. Hammer, M. E. Glinsky, W. L. Kruer, S. C. Wilks, J. Woodworth, E. M. Campbell, M. D. Perry, and R. J. Mason, Phys. Plasmas **1**, 1626 (1994).

[12]R. Kodama, P. A. Norreys, K. Mima, A. E. Dangor, R. G. Evans, H. Fujita, Y. Kitagawa, K. Krushelnick, T. Miyakoshi, N. Miyanaga et al., Nature **412**, 798 (2001).

[13]M. Roth, T. E. Cowan, M. H. Key, S. P. Hatchett, C. Brown, W. Fountain, J. Johnson, D. M. Pennington, R. A. Snavely, S. C. Wilks et al., Phys. Rev. Lett. **86**, 436 (2001).

[14]V. Malka, S. Fritzler, E. Lefebvre, E. d'Humières, R. Ferrand, G. Grillon, C. Albaret, S. Meyroneinc, J. P. Chambaret, A. Antonetti et al., Med. Phys. **31**, 1587 (2004).

[15]T. Sokollik, M. Schnürer, S. Ter-Avetisyan, P. V. Nickles, E. Risse, M. Kalashnikov, W. Sandner, G. Priebe, M. Amin, T. Toncian et al., Appl. Phys. Lett. **92**, 091503 (2008).

[16]S. Fritzler, V. Malka, G. Grillon, J. P. Rousseau, F. Burgy, E. Lefebvre, E. d'Humières, P. McKenna, and K. W. D. Ledingham, Appl. Phys. Lett. **83**, 3039 (2003).

[17]P. Gibbon and E. Förster, Plasma Phys. Controlled Fusion **38**, 769 (1996).

[18]A. Macchi, M. Borghesi, and M. Passoni, Rev. Mod. Phys. **85**, 751 (2013).

[19]H. Daido, M. Nishiuchi, and A. S. Pirozhkov, Rep. Prog. Phys. **75**, 056401 (2012).

[20]T. E. Cowan, J. Fuchs, H. Ruhl, A. Kemp, P. Audebert, M. Roth, R. Stephens, I. Barton, A. Blazevic, E. Brambrink et al., Phys. Rev. Lett. **92**, 204801 (2004).

[21]H. Schwoerer, S. Pfotenhauer, O. Jäckel, K.-U. Amthor, B. Liesfeld, W. Ziegler, R. Sauerbrey, K. W. D. Ledingham, T. Esirkepov et al., Nature **439**, 445 (2006).

[22]S. Tata, A. Mondal, S. Sarkar, J. Jha, Y. Ved, A. D. Lad, J. Colgan, J. Pasley, and M. Krishnamurthy, Phys. Rev. Lett. **121**, 134801 (2018).

[23]M. M. Murnane, H. C. Kapteyn, S. P. Gordon, J. Bokor, E. N. Glytsis, and R. W. Falcone, Appl. Phys. Lett. **62**, 1068 (1993).

[24]V. Kaymak, E. Aktan, M. Cerchez, B. Elkin, M. Papenheim, R. Prasad, A. Pukhov, H. C. Scheer, A. Schroer, O. Willi, and B. Aurand, Sci. Rep. **9**, 18672 (2019).

[25]D. Margarone, O. Klimo, I. J. Kim, J. Prokůpek, J. Limpouch, T. M. Jeong, T. Mocek, J. Pšikal, H. T. Kim, J. Prôška, K. H. Nam, L. Štolcová, I. W. Choi, S. K. Lee, J. H. Sung, T. J. Yu, and G. Korn, Phys. Rev. Lett. **109**, 234801 (2012).

[26]M. Passoni, A. Sgattoni, I. Prencipe, L. Fedeli, D. Dellasega, L. Cialfi, I. Woo Choi, I. J. Kim, K. A. Janulewicz, H. Woon Lee, J. H. Sung, S. K. Lee, and C. H. Nam, Phys. Rev. Accel. Beams **19**, 061301 (2016).

[27]D. Khaghani, M. Lobet, B. Borm, L. Burr, F. Gärtner, L. Gremillet, L. Movsesyan, O. Rosmej, M. E. Toimil-Molares, F. Wagner, and P. Neumayer, Sci. Rep. **7**, 11366 (2017).

[28]G. Kulcsar, D. AlMawlawi, F. W. Budnik, P. R. Herman, M. Moskovits, L. Zhao, and R. S. Marjoribanks, Phys. Rev. Lett. **84**, 5149 (2000).

[29]S. P. Gordon, T. Donnelly, A. Sullivan, H. Hamster, and R. W. Falcone, Opt. Lett. **19**, 484 (1994).

[30]A. Macchi, Phys. Plasmas **25**, 031906 (2018).

[31]M. Krishnamurthy, S. Mondal, A. D. Lad, K. Bane, S. Ahmed, V. Narayanan, R. Rajeev, G. Chatterjee, P. K. Singh, G. R. Kumar et al., Opt. Express **20**, 5754 (2012).

[32]M. Dalui, M. Kundu, T. M. Trivikram, R. Rajeev, K. Ray, and M. Krishnamurthy, Sci. Rep. **4**, 6002 (2014).

[33]M. Dalui, M. Kundu, T. M. Trivikram, K. Ray, and M. Krishnamurthy, Phys. Plasmas **23**, 103101 (2016).

[34]M. Murakami and K. Mima, Phys. Plasmas **16**, 103108 (2009).

[35]M. Murakami and M. Tanaka, Appl. Phys. Lett. **102**, 163101 (2013).

[36]M. A. H. Zosa and M. Murakami, Phys. Plasmas **27**, 033103 (2020).

[37]S. Tata, A. Mondal, S. Sarkar, A. M. Lad, and M. Krishnamurthy, Rev. Sci. Instrum. **88**, 083305 (2017).

[38]R. Rajeev, K. P. M. Rishad, T. M. Trivikram, V. Narayanan, and M. Krishnamurthy, Rev. Sci. Instrum. **82**, 083303 (2011).

[39]G. Qi, Y. Wang, L. Estevez, A. K. Switzer, X. Duan, X. Yang, and E. P. Giannelis, Chem. Mater. **22**, 2693 (2010).

[40]T. Kluge, T. Cowan, A. Debus, U. Schramm, K. Zeil, and M. Bussmann, Phys. Rev. Lett. **107**, 205003 (2011).